

Binarization-Aware Adjuster: A Theoretical Framework for Bridging Continuous Optimization and Discrete Inference with Application to Edge Detection

Hao Shu*

Sun-Yat-Sen University, Shenzhen, China

Shenzhen University, Shenzhen, China

Abstract

In machine learning, discrete decision-making tasks exhibit a fundamental inconsistency between training and inference: models are optimized using continuous-valued outputs, yet evaluated through discrete predictions. This discrepancy arises from the non-differentiability of discretization operations, weakening the alignment between optimization objectives and practical decision outcomes. To address this, we present a theoretical framework for constructing a Binarization-Aware Adjuster (BAA) that integrates binarization behavior directly into gradient-based learning. Central to the approach is a Distance Weight Function (DWF) that dynamically modulates pixel-wise loss contributions based on prediction correctness and proximity to the decision boundary, thereby emphasizing decision-critical regions while de-emphasizing confidently correct samples. Furthermore, a self-adaptive threshold estimation procedure is introduced to better match optimization dynamics with inference conditions. As one of its applications, we implement experiments on the edge detection (ED) task, which also demonstrate the effectiveness of the proposed method experimentally. Beyond binary decision tasks and ED, the proposed framework provides a general strategy for aligning continuous optimization with discrete evaluation and can be extended to multi-valued decision processes in broader structured prediction problems.

*
Email address: Hao_B_Shu@163.com (Hao Shu)

Keywords: Adjusted Loss Function, Binarization-Aware Adjuster, Distance Weight Function, Continuous-Discrete Alignment, Edge Detection

1. Introduction

Many real-world vision tasks, such as semantic segmentation, image classification, object recognition, and edge detection (ED) [1, 2, 3, 4, 5], ultimately require discrete decisions (e.g., binary or categorical outputs). However, learning methods, such as deep neural networks, constrained by the need for differentiable computation, are typically optimized using continuous-valued loss functions within gradient-based learning frameworks [6, 7, 8, 9, 10]. As non-differentiable inference operations, such as thresholding, quantization, or category assignment, are excluded from the optimization process, a fundamental gap arises between continuous-valued optimization during training and the discrete inference deployed at test time. This gap may lead to suboptimal performance, as optimization does not always align with decision-critical behavior.

This mismatch is particularly evident in pixel-level binary prediction tasks. For example, edge detection (ED) aims to generate binary edge maps but is typically trained using continuous-valued loss functions such as binary cross-entropy (BCE). Since binarization is non-differentiable, it is excluded from the optimization loop and applied only post hoc during evaluation. As a result, model updates tend to prioritize pixels that are easy to optimize but have limited influence on the binary output, whereas pixels near the decision boundary, which are more critical for final accuracy, receive insufficient emphasis due to their lower weights and higher optimization difficulty.

Several studies have attempted to mitigate the inconsistency between decision behavior and training objectives, typically by changing losses that rebalance decision classes, such as weighted BCE [11] or alternative ones [12, 13]. However, to the best of our knowledge, few existing methods explicitly integrate binarization (or discretization) behavior into gradient-based optimization, leaving the fundamental optimization–inference misalignment unresolved.

To address this issue, we propose a theoretically grounded framework named *Binarization-Aware Adjuster* (BAA), which explicitly embeds binarization behavior into the opti-

mization process. The core idea is a threshold-aware loss adjustment mechanism based on the proposed *Distance Weight Function* (DWF), which dynamically reweights pixel-level loss according to prediction correctness and proximity to the decision threshold. This enables the model to allocate greater learning capacity to decision-critical regions while down-weighting confidently correct predictions that exert limited influence on binary outputs. Additionally, a self-adaptive threshold estimation strategy is introduced to align the adjuster with inference behavior. Since the BAA is continuous and differentiable, it can be seamlessly incorporated into existing gradient-based optimization pipelines, allowing discrete inference behavior to influence learning directly.

The proposed framework is designed for binary decision tasks and is applied to the ED task to demonstrate its effectiveness. ED is selected as a representative implementation scenario due to its foundational role in low-level vision and its strong dependence on precise decision boundaries. Furthermore, many structured prediction tasks can be viewed as extensions or generalizations of the ED paradigm. Binary decision tasks are selected since they can display our method most conveniently and clearly. Nevertheless, the proposed BAA mechanism is conceptually extensible to multi-value discrete decision tasks and applicable to a broader range of tasks involving discrete decisions, such as segmentation, classification, and object recognition.

The main contributions of this work are summarized as follows:

- We identify a fundamental mismatch between continuous optimization and discrete inference in model training and propose the Binarization-Aware Adjuster (BAA) framework to bridge this gap.
- We develop a principled formulation based on the Distance Weight Function (DWF), enabling binarization-aware loss adjustment while retaining full differentiability.
- We apply the proposed framework to the edge detection task and implement extensive experiments on substantial benchmark datasets across multiple architectures.

2. Previous Works

A large number of learning-based systems perform discrete decision-making while being optimized using continuous-valued loss functions. This discrepancy has motivated studies on improving the alignment between continuous optimization during training and discrete evaluation at inference. In this work, edge detection (ED) is adopted as an illustrative validation scenario due to its strong dependency on binary decisions and its relevance to many structured prediction tasks. In the following, we briefly review related studies with ED as a representative example.

2.1. Datasets

Historically, early vision research commonly relied on general-purpose datasets. For instance, BSDS300/500 [14] have been used in contour detection, segmentation, and ED. Common datasets such as PASCAL VOC [15], COCO [16], and NYUD [17] have been widely adopted across segmentation, detection, and image classification tasks. With increasing task specialization, dataset selection became more focused, e.g., PASCAL VOC for object detection, NYUD for segmentation, and BSDS500 for contour-based analysis.

For ED specifically, dedicated datasets were developed to provide more accurate edge annotations. BIPED/BIPED2 [18] offers edge annotations for 250 high-resolution campus images, BRIND [6] extended BSDS500 with reannotated edge labels, and UDED [19] provides carefully selected high-quality samples.

Despite these efforts, annotation quality remains a major challenge. Human-labeled edge maps often suffer from inconsistency, ambiguity, and noise. Although robust training strategies and refined labeling protocols have been proposed [20, 21, 22], annotation noise still affects both generalization ability and fair benchmarking.

2.2. Model Architectures

Deep learning architectures have achieved broad success in computer vision [23], natural language processing [24], and decision systems [25]. Major architectural paradigms, including convolutional neural networks (CNNs), transformer models, and diffusion-based methods, have demonstrated significant cross-domain applicability.

Using ED as an example, the pioneering work HED [11] validated the effectiveness of multi-scale deep supervision using CNNs, outperforming traditional approaches [4, 5] and early feature-based learning methods [26, 27, 28, 29, 30]. Subsequent works, such as RCF [31], BDCN [32], PiDiNet [33], and DexiNet [34], further optimized fusion strategies and model structures. Transformer-based [7, 35] and diffusion-based [8, 9] designs have also been explored. More recently, the Extractor–Selector framework [10] demonstrated improvements through refined feature selection. Among these approaches, CNN-based models remain the most widely adopted due to their robustness and maturity.

2.3. Loss Functions

Loss function design is critical in model optimization. Binary cross-entropy (BCE) was initially the standard for decision tasks. However, BCE assigns equal importance to positive and negative samples, which is unsuitable for imbalanced data. To address this, Weighted BCE (WBCE) is widely adopted and still the most standard one currently. Other alternatives include Dice loss [36] and tracing loss [37] for geometry-aware optimization, AP-loss [38] and RankED [12] based on ranking formulation, and SWBCE [13] that models uncertainty in manual annotations.

Although these methods improve sample weighting, they generally do not explicitly model the final inference rule, leaving the discretization step separate from the optimization process. Consequently, the fundamental continuous–discrete gap remains unresolved. This limitation motivates the development of our BAA framework.

2.4. Evaluation Metrics

For binary decision tasks, performance is typically evaluated using the $F\beta$ score:

$$F\beta = \frac{(1 + \beta^2) \times \text{Precision} \times \text{Recall}}{\beta^2 \times \text{Precision} + \text{Recall}}, \quad (1)$$

where

$$\text{Precision} = \frac{TP}{TP + FP}, \quad \text{Recall} = \frac{TP}{TP + FN}. \quad (2)$$

Here, TP denotes true positives, FP false positives, and FN false negatives, with β typically set to 1. The most frequently used metrics include:

- **ODS (Optimal Dataset Score):** Best F_1 using a single threshold for the entire dataset.
- **OIS (Optimal Image Score):** Mean of each image’s best F_1 using image-specific thresholds.

For ED, the commonly used metric computation was proposed in [26] with error tolerance to compensate for minor spatial deviations. Recent studies [22] recommend stricter and standardized tolerance settings for more reliable comparison.

3. Methodology: General Theory

This section presents the theoretical framework of our method. Here, the design for binary decision tasks is proposed for illustrative convenience and simplicity. Note that the discussions can be easily extended to multi-value discrete decision tasks.

3.1. Motivation and Insight

A key challenge in training binary decision models is the mismatch between training objectives and evaluation protocols. During training, models generate continuous-valued outputs, typically normalized to $[0,1]$, and are optimized using pixel-wise loss functions such as WBCE. In contrast, evaluation metrics are computed on binarized maps, obtained by applying a fixed threshold to these outputs. Since the binarization operation is discontinuous, it cannot be directly incorporated into the training process. This disconnect creates a fundamental issue: the loss function does not explicitly align with the discrete classification decisions that ultimately determine evaluation performance.

This gap introduces a critical inefficiency in optimization. Pixels whose predicted values lie on the correct side and far from the decision threshold, namely those correct pixels with high confidence, tend to dominate the gradient signal since they are easy to optimize. In contrast, pixels with predictions near the threshold, which are more ambiguous and critical to classification, contribute less to the gradients since they are more difficult to optimize. Consequently, the optimizer, driven by gradient magnitude, inadvertently prioritizes ‘easy’ but less effective pixels over ‘ambiguous’ but crucial

ones, due to the nature of the optimization that tends to optimize the less-challenging pixels with higher priority. This misallocation of optimization effort can prevent the optimal parameter from being learned, resulting in suboptimal learning and degraded final performance.

For example, Table 1 reports optimal binarization thresholds for various ED models on multiple datasets under WBCE loss, which typically fall between 0.6 and 0.8. Suppose the binarization threshold is 0.7, then reducing the predicted value of a non-edge pixel from 0.50 to 0.01 has no effect on the final binary edge map, but it significantly reduces the loss. Moreover, such confident-correct predictions are often easy to optimize, which is the reason that they become the correctly predicted ones with high confidence. Therefore, training naturally prioritizes them for their optimization ease since they contribute more to loss, even though further improvement on them yields no benefit for the final decision. In contrast, increasing the predicted value of an edge pixel from 0.69 to 0.71 can be more difficult, which is the reason why its prediction is near the decision threshold. Therefore, though critical for correct classification, it contributes less to the loss and thus is more easily overlooked.

Table 1

Optimal binarization thresholds under WBCE training for ED models: Evaluation uses 1-pixel error tolerance without NMS. Experimental settings follow the ones in Section 4.1. Models are retrained on the pre-training set and evaluated on the validation set.

	UDED	BSDS500	BRIND	BIPED2
HED	0.74	0.85	0.77	0.79
BDCN	0.65	0.79	0.78	0.72
Dexi	0.63	0.87	0.79	0.79
EES3-Double	0.61	0.86	0.77	0.80

To bridge the continuous optimization and the binarization inference, we propose a novel loss adjustment mechanism, realized by a BAA, that dynamically re-weights pixel-wise loss contributions based on both proximity to the decision threshold and

classification correctness. By explicitly incorporating binarization behavior into the training process, the BAA method ensures that the model allocates its learning capacity to the most decision-critical pixels.

3.2. Adjusted Loss Function Formulation

Although designing the BAA is non-trivial, the idea of using it is conceptually simple. Let us first address the simpler task, formally defining the adjusted loss function in this subsection, and leave the more challenging part, designing the BAA, to the next.

We define an adjusted loss as a loss that incorporates a pixel-wise weighting factor:

$$L_{Adj,\delta}(Pred, Gt) = \sum_i (Adj(Pred_i, Gt_i) + \delta)L(Pred_i, Gt_i) \quad (3)$$

where i runs over all pixels, L is a selected baseline pixel-wise loss function such as WBCE¹, $Pred$ and Gt represent the model prediction and the ground truth, respectively, $Pred_i$ and Gt_i represent the model prediction and the ground truth of the i -th element, respectively, and $\delta \geq 0$ is a pre-defined hyperparameter, directly adding loss L with intensity δ to the loss to stabilize training. The function Adj is called an **Adjuster**, where $Adj(Pred_i, Gt_i) \in [0, 1]$ assigns dynamic weights, emphasizing the training signal according to the pixel’s contribution to the final binary decision.

Despite the simple idea, the problem lies in the design of the adjuster. A naive choice of $Adj(Pred_i, Gt_i)$ is the binary mask $\hat{Adj}_{thr}(Pred_i, Gt_i)$, defined as:

$$\hat{Adj}_{thr}(Pred_i, Gt_i) = \begin{cases} 0 & \text{If } (Pred_i - thr)(Gt_i - thr) \geq 0 \\ 1 & \text{Otherwise} \end{cases} \quad (4)$$

where thr is the binarization threshold. Hence, $L_{Adj,\delta}$ satisfying (providing $\delta = 0$):

- If an element is correctly classified, then the loss on it is 0.
- If an element is incorrectly classified, then the loss on it is positive.

¹The same symbol L is employed to denote both the loss function on a single element such as a pixel ($L(Pred_i, Gt_i)$) and on the whole object such as images ($L(Pred, Gt)$).

This adjuster emphasizes only misclassified elements. However, the discontinuity of its corresponding adjusted loss function renders it unsuitable for gradient-based optimization. Therefore, a smoother, differentiable formulation is necessary.

3.3. Design of the Binarization-Aware Adjuster

Let thr denote the binarization threshold. The adjuster Adj we aim to construct should satisfy:

- *C1 (Continuity)*: The adjuster Adj must be continuous to allow gradient-based optimization.
- *C2 (Non-negativity)*, $Adj(Pred_i, Gt_i)$ should be non-negative since it represents the weight of an element. Without loss of generality, assume that $Adj(Pred_i, Gt_i) \in [0, 1]$, since multiplying a constant provides no essential difference.
- *C3 (Uncertainty Emphasis)*: If an element is correctly classified, then the closer the prediction is to thr , the higher the weight $Adj(Pred_i, Gt_i)$ of it should be, reflecting the loss caused by the uncertainty.
- *C4 (Confidence Saturation)*: If a n element is correctly classified with high confidence (i.e., prediction far from thr), then $Adj(Pred_i, Gt_i)$ should decay to 0 quickly as $Pred_i$ goes away from thr , representing that further optimizing provide little benefits. Indeed, $Adj(Pred_i, Gt_i)$ should close to the maximal value when $Pred_i$ is close to thr , remain large when $Pred_i$ is not far from thr , and decay to 0 after some pre-defined distance thr_dev .
- *C5 (Classification Sensitivity)*: If an element is misclassified, for example if it is an edge one but $Pred_i < thr$ or is a non-edge one but $Pred_i \geq thr$ in the ED task, its weight $Adj(Pred_i, Gt_i)$ should be maximal, representing correctly classification is of the first priority.

These conditions ensure that misclassified elements always receive full attention, and optimization of correct elements is focused on the uncertain parts while conserving effort on highly confident correct parts. We call an adjuster satisfying the above conditions a ***Binarization-Aware Adjuster***, abbreviated as ***BAA*** for short. Namely:

Definition 1. A *Binarization-Aware Adjuster (BAA)* regarding $thr \in [0, 1]$ and $thr_dev > 0$ is a function valued at $[0, 1]$ satisfying the above conditions C1 to C5.

Let thr_dev denote the threshold window from C4. To construct a BAA, we define:

Definition 2. A function $f_{thr_dev}(x)$ is said to be a *Distance Weight Function (DWF)* regarding the threshold window $thr_dev \in \mathbb{R}_+$, if it satisfies the following properties:

- *Continuity:* $f_{thr_dev}(x) : [0, thr_dev] \rightarrow [0, 1]$ is continuous.
- *Monotonically Decreasing:* $f_{thr_dev}(x_1) \leq f_{thr_dev}(x_2)$, $\forall x_1, x_2 \in [0, thr_dev]$ with $x_1 \geq x_2$. (or equivalently, $\frac{df_{thr_dev}}{dx}(x) \leq 0$ for differentiable $f_{thr_dev}(x)$).
- *Concavity:* $f(\lambda x_1 + (1 - \lambda)x_2) \geq \lambda f(x_1) + (1 - \lambda)f(x_2)$, $\forall x_1, x_2 \in [0, thr_dev]$ and $\lambda \in [0, 1]$. (or equivalently, $\frac{d^2 f_{thr_dev}}{dx^2}(x) \leq 0$ for secondary differentiable $f_{thr_dev}(x)$).
- *Boundary Conditions:* $f_{thr_dev}(0) = 1$, and $f_{thr_dev}(thr_dev) = 0$.

Then:

$$\bar{Adj}(Pred_i, Gt_i) = \begin{cases} f_{thr_dev}(|Pred_i - thr|) & 0 \leq |Pred_i - thr| \leq thr_dev \\ 0 & |Pred_i - thr| > thr_dev \end{cases} \quad (5)$$

satisfies C1 – C4.

An example of the DWF $f_{thr_dev}(x) = f_{b,thr_dev}(x)$ can be constructed as:

$$f_{b,thr_dev}(x) = \frac{e^{b \times x} - e^{b \times thr_dev}}{1 - e^{b \times thr_dev}} \quad (6)$$

where $b \geq 0$ is pre-defined, controlling the decay rate.

To also meet C5, we define the masked distance as:

Definition 3. The $([0, 1])$ masked distance $MD_{thr}(x, y) : [0, 1]^2 \rightarrow [0, 1]$ regarding the threshold $thr \in [0, 1]$ is defined as:

$$MD_{thr}(x, y) = (x - thr) \times y + (thr - x) \times (1 - y) \quad (7)$$

Hence, $MD_{thr}(Pred_i, Gt_i)$ measures both the correctness and confidence of the element i . For a wrongly predicted element i , namely whose prediction is on the different side of the thr as its ground truth value, $MD_{thr}(Pred_i, Gt_i) \leq 0$, while for a correctly predicted element i , $MD_{thr}(Pred_i, Gt_i)$ is the L^1 distance of $Pred_i$ from the binarization threshold thr .

Now, a BAA can be defined as:

$$BAA_{thr,thr_dev}(Pred_i, Gt_i) = \hat{f}_{thr_dev}(MD_{thr}(Pred_i, Gt_i)) \quad (8)$$

where \hat{f}_{thr_dev} is an extension of a selected DWF $f_{thr_dev}(x)$, defined as:

$$\hat{f}_{thr_dev}(x) = \begin{cases} 1 & x < 0 \\ f_{thr_dev}(x) & 0 \leq x \leq thr_dev \\ 0 & x > thr_dev \end{cases} \quad (9)$$

3.4. Theoretical Properties of the BAA

To better understand the proposed adjuster's behavior, we analyze its mathematical properties. Let $f_{thr_dev}(x) = f_{b,thr_dev}(x)$ be defined as in Equations 6 and $\hat{f}_{thr_dev}(x) = \hat{f}_{b,thr_dev}(x)$ be its extension defined in Equation 9. Then $\hat{f}_{b,thr_dev}(x)$ serves as a smooth approximation to a hard binarization function. Specifically, it generalizes the discrete threshold-based binary weighting function $B_{thr_dev}(x)$ on threshold thr_dev , defined as:

$$B_{thr_dev}(x) = \begin{cases} 1 & x < thr_dev \\ 0 & x \geq thr_dev \end{cases} \quad (10)$$

The two functions coincide as $b \rightarrow +\infty$:

$$\lim_{b \rightarrow +\infty} \hat{f}_{b,thr_dev}(x) = B_{thr_dev}(x) \quad (11)$$

Therefore, \hat{f}_{b,thr_dev} is a continuous approximation for threshold logic. Accordingly, the $BAA_{thr,thr_dev}(Pred_i, Gt_i) = BAA_{thr,b,thr_dev}(Pred_i, Gt_i)$, defined by Equation 8, converges to a discrete decision-based adjuster $\widetilde{Adj}_{thr,thr_dev}(Pred_i, Gt_i)$, defined as:

$$\widetilde{Adj}_{thr,thr_dev}(Pred_i, Gt_i) = \begin{cases} 0 & (Pred_i - thr)(Gt_i - thr) \geq 0 \ \& \ |Pred_i - thr| \geq thr_dev \\ 1 & \text{Otherwise} \end{cases} \quad (12)$$

i.e.,

$$\lim_{b \rightarrow +\infty} BAA_{thr,b,thr_dev}(Pred_i, Gt_i) = \widetilde{Adj}_{thr,thr_dev}(Pred_i, Gt_i) \quad (13)$$

This confirms that the BAA bridges the binarization logic with the continuous-loss gradient-based training. Furthermore, let also $thr_dev \rightarrow 0^+$, then it is reduced to \hat{Adj}_{thr} from Equation 4.

Moreover, for a DWF $f_{thr_dev}(x)$, the following bounds holds:

$$1 - \frac{x}{thr_dev} \leq f_{thr_dev}(x) \leq 1 \quad (14)$$

Therefore:

$$\lim_{thr_dev \rightarrow +\infty} f_{thr_dev}(x) = 1 \quad (15)$$

which implies that:

$$\lim_{thr_dev \rightarrow +\infty} BAA_{thr,thr_dev}(x) = 1 \quad (16)$$

and the adjusted loss $L_{Adj,\delta}$ defined in Equation 3 degenerates to the baseline loss L up to a constant:

$$\lim_{thr_dev \rightarrow \infty} L_{Adj,\delta}(Pred, Gt) = (1 + \delta)L(Pred, Gt) \quad (17)$$

In summary, the proposed adjusted loss function $L_{Adj,\delta}$ with $Adj = BAA_{thr,b,thr_dev}$ defined above by the DWF in Equation 6, generalizes the baseline loss L . It degenerates to the baseline loss when $thr_dev \rightarrow +\infty$, converges to a binary weighted loss when $b \rightarrow +\infty$, and maintains the continuity². These asymptotic behaviors confirm that the constructed BAA bridges the continuous loss and post-binarization classification, aligning training with downstream evaluation.

3.5. Hyperparameter Selection and Training Protocol

The proposed BAA depends on three hyperparameters: thr : binarization threshold, thr_dev : threshold window beyond which correct predictions are ignored in optimization, and b (when employing $f_{b,thr_dev}(x)$ from Equation 6 as the DWF): DWF decay rate,

²Here, $\delta = 0$ is provided.

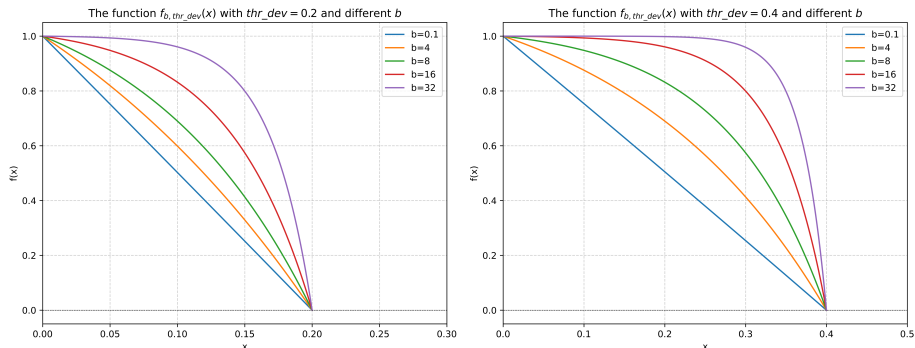


Figure 1 The different choices of b in the DWF $f_{b,thr_dev}(x)$ presented in Equation 6

The DWF decay rate b occurs specifically in the DWF defined in Equation 6, controlling the concavity of $f_{b,thr_dev}(x)$, determining how sharply the adjusted weight decays as predictions diverge from the decision boundary thr . Its effect is illustrated in Figure 1, and we set $b = 16$ as the default.

thr_dev defines the margin around thr within which a correct prediction is considered uncertain. A correct prediction with $|Pred_i - thr| > thr_dev$ is considered as confidently correct and receives zero weight. We empirically choose $thr_dev = 0.2$ for the ED task.

thr is the most critical hyperparameter in the BAA. For ED models, experiments (Table 1) show that the optimal value typically lies between 0.6 and 0.8, so we use $thr = 0.7$ as the default.

However, given its importance, it is worth providing a calibration method for it. Specifically, we suggest a self-adaptive thr chosen by pre-training: pre-train the model on a sub-dataset without applying BAA and evaluate the pre-trained model on a validation set to select a suitable thr for BAA.

Therefore, the final training protocol of a model M under a selected baseline loss function L on a dataset D , with the presented BAA method, can be formulated as:

- Step 1: Split D into pre-train set P , validation set V , and test set T .
- Step 2: Train M on P using baseline loss L , and evaluate on V to estimate thr .
- Step 3: Retrain M via $L_{BAA,\delta}$, on $P \cup V$, and evaluate finally on T .

In experiments, δ is simply set to be 1.

4. Experiment: Application to Edge Detection

To validate the effectiveness of the proposed BAA framework, we apply it to the ED task, which is selected since it is one of the most fundamental tasks in computer vision, supporting substantial high-level tasks, and many tasks can be reformulated to it.

4.1. Experimental Setting

We adopt the adjuster designed by Equation 6, 7, 8, and 9 as the BAA, and WBCE as the baseline loss function L , due to its widespread use in ED tasks.

4.1.1. Baseline and Benchmark

The proposed method is evaluated across a range of ED models, including: HED (2015) [11], BDCN (2022) [32], Dexi (2023) [34], and EES3-Double (2025) [10], the EES framework integrating the above three models with the double-size selector. Experiments are conducted on four benchmark datasets: BRIND [6], BSDS500 [14], UDED [19], and BIPED2 [18].

All models are retrained from scratch on each dataset to ensure fairness. For consistency and simplicity, only the final output of each model is used for supervision, bypassing any need for hyperparameter tuning in intermediate layers. Each model is trained under the following three configurations of loss function for comparison:

- Standard WBCE (baseline).
- WBCE with a fixed-threshold BAA using $thr = 0.7$ (denoted as *BAA-0.7*)
- WBCE with a self-adaptive adjuster where thr is automatically selected following the method in Section 3.5 (denoted as *BAA-SA*).

Unless otherwise specified, the hyperparameters for the adjusted loss defined by the BAA are fixed at $thr_{dev} = 0.2$, $b = 16$, and $\delta = 1$.

Evaluation protocols follow the standard ED metrics (ODS and OIS) introduced in [26], under the strictest 1-pixel error tolerance without post-processing techniques such as non-maximal suppression (NMS), suggested in [22]. The evaluations under the traditional relaxed error tolerance (4.3 to 11.1 pixels) with NMS are provided in the appendix.

4.1.2. Dataset Partitions and Augmentation

Dataset preprocessing and postprocessing procedures follow those introduced in [10]. Details are stated as follows.

The dataset partitions follow: BRIND and BSDS500: 400 training images and 100 testing images, UDED: 20 training images and 7 testing images (excluding two images with resolution below 320×320), and BIPED2: 200 training images and 50 testing images.

For training under the self-adaptive adjuster setting in section 3.5, each training set is further divided into pre-training and validation subsets, following: BRIND and BSDS500: 300 pre-training and 100 validation images, UDED: 15 pre-training and 5 validation images, and BIPED2: 150 pre-training and 50 validation images.

Data augmentations are applied, including: Halving the images until both height and width are strictly below 640 pixels, rotations at four angles, 0° , 90° , 180° , and 270° , with horizontal flips, as well as addition of noiseless data.

4.1.3. Training Note

During training, input images are randomly cropped to 320×320 and refreshed every 5 epochs. The batch size is set to 8. All models are trained on an A100 GPU using Adam optimizer, with a learning rate of 0.0001 and a weight decay of 10^{-8} .

Training runs for 200 epochs on UDED and 50 epochs on the remaining datasets.

4.1.4. Inference Method

In the inference phase, each image is split into overlapping 320×320 patches with a stride of 304 pixels (i.e., 16 pixels overlap). The model predicts edge maps on each patch independently, and the outputs are aggregated to form the final edge map.

Further implementation details can be found in the code or in [10].

4.2. Experimental Results

Tables 2 and 3 report the ED performance of all methods on BRIND, BSDS500, UDED, and BIPED2 datasets under the strict 1-pixel error tolerance setting, without applying NMS. The evaluation includes ODS and OIS scores for each configuration.

The results clearly demonstrate that incorporating the proposed BAA method, whether with the fixed threshold (*BAA-0.7*) or the self-adaptive strategy (*BAA-SA*), leads to improvements in performance across most models and datasets.

Both variants of the BAA loss improve the baseline WBCE loss across all models and datasets. The self-adaptive version (*BAA-SA*) tends to achieve slightly better performance than the fixed threshold in most cases.

On BRIND, the best ODS gains are observed in BDCN (about +1.5%) using the self-adaptive adjuster (*BAA-SA*). On BSDS500, EES3-Double and BDCN benefit most from the adjuster, with ODS improvements up to +1.8% and +2.6%, respectively. UDED shows the most significant performance gains. The average ODS improves by about +2.7% (*BAA-0.7*) and +2.4% (*BAA-SA*) compared to the baseline. On BIPED2, the improvements are modest but consistent with *BAA-SA* outperforming both baseline and fixed-threshold setups.

These results strongly validate the effectiveness of the proposed BAA method, especially the self-adaptive variant. The method is robust across different backbone architectures and datasets, offering consistent improvements with minimal modifications to the existing training pipeline.

4.3. Ablation Study

Figure 2 illustrates how ODS and OIS scores vary with different values of *thr_dev* (from 0.1 to 0.7) and decay rates *b* (8, 16, 32) in the DWF (Equation 6). All experiments are conducted on the BRIND dataset using the EES3-Double model trained with the BAA-WBCE loss. The threshold *thr* is fixed at 0.7, and δ at 1.

This ablation study shows that across all tested configurations, *thr_dev* = 0.2 consistently yields the best performance. Also, the proposed BAA method is robust to a wide range of hyperparameter settings, which simplifies hyperparameter tuning and reinforces the general applicability of the method.

Table 2

Results on BRIND and BSDS500 under 1-pixel error tolerance without NMS: For BRIND, all annotations per image are merged into a single binary ground truth map, where a pixel is considered an edge one if it is marked as such by any annotator. For BSDS500, only label 1 is used as the ground truth. Notations follow those introduced in the main-text. The best scores for each model are highlighted in **bold**. Rows labeled *A-No-BAA*, *A-BAA-0.7*, and *A-BAA-SA* represent the average performance across the four models corresponding to each setting, respectively, while *Improvement* rows indicate the relative improvements over the baseline.

	BRIND		BSDS500	
	ODS	OIS	ODS	OIS
HED (2015)	0.664	0.673	0.444	0.455
HED-BAA-0.7	0.668	0.676	0.441	0.453
HED-BAA-SA	0.664	0.672	0.455	0.465
BDCN (2022)	0.655	0.663	0.432	0.446
BDCN-BAA-0.7	0.662	0.671	0.445	0.452
BDCN-BAA-SA	0.665	0.674	0.454	0.468
Dexi (2023)	0.675	0.683	0.465	0.473
Dexi-BAA-0.7	0.674	0.683	0.475	0.485
Dexi-BAA-SA	0.679	0.687	0.470	0.480
EES3-Double (2025)	0.683	0.690	0.488	0.504
EES3-Double-BAA-0.7	0.690	0.697	0.493	0.509
EES3-Double-BAA-SA	0.690	0.697	0.497	0.507
A-No-BAA	0.669	0.677	0.457	0.470
A-BAA-0.7	0.674	0.682	0.464	0.475
A-BAA-0.7-Improvement	+0.75%	+0.74%	+1.53%	+1.06%
A-BAA-SA	0.675	0.683	0.469	0.480
A-BAA-SA-Improvement	+0.90%	+0.89%	+2.63%	+2.13%

Table 3

Results on UDED and BIPED2 under 1-pixel error tolerance without NMS: Notations follow the ones in Table2.

	UDED		BIPED2	
	ODS	OIS	ODS	OIS
HED (2015)	0.709	0.742	0.630	0.633
HED-BAA-0.7	0.727	0.755	0.629	0.634
HED-BAA-SA	0.712	0.748	0.633	0.635
BDCN (2022)	0.688	0.723	0.636	0.639
BDCN-BAA-0.7	0.713	0.741	0.637	0.639
BDCN-BAA-SA	0.712	0.749	0.640	0.643
Dexi (2023)	0.700	0.738	0.643	0.648
Dexi-BAA-0.7	0.721	0.752	0.640	0.646
Dexi-BAA-SA	0.731	0.765	0.641	0.646
EES3-Double (2025)	0.751	0.780	0.670	0.673
EES3-Double-BAA-0.7	0.762	0.794	0.671	0.675
EES3-Double-BAA-SA	0.758	0.791	0.675	0.680
A-No-BAA	0.712	0.746	0.645	0.648
A-BAA-0.7	0.731	0.761	0.644	0.649
A-BAA-0.7-Improvement	+2.67%	+2.01%	-0.16%	+0.15%
A-BAA-SA	0.729	0.763	0.647	0.651
A-BAA-SA-Improvement	+2.39%	+2.28%	+0.31%	+0.46%

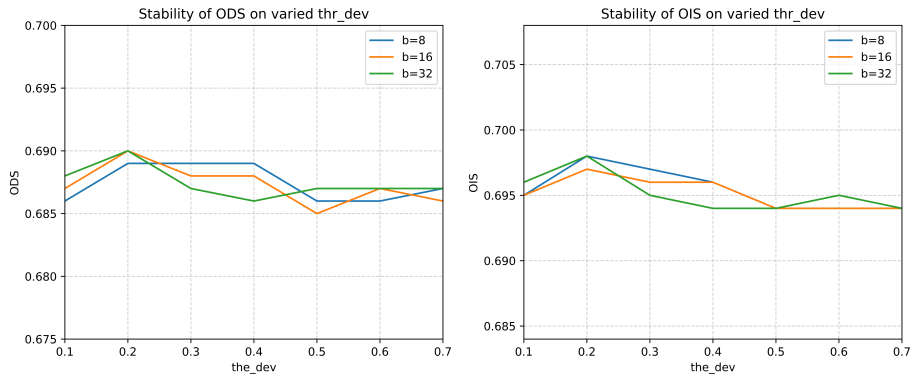


Figure 2 ODS and OIS across thr_dev : Figures show how ODS and OIS vary with thr_dev values from 0.1 to 0.7, across different decay rates b (8, 16, 32). Experiments are conducted on BRIND using the EES3-Double model and adjusted WBCE loss. Threshold thr is fixed at 0.7 and δ at 1.

5. Discussion

Although the BAA is initially designed for binary decision tasks, its formulation can be naturally extended to general multi-valued discrete inference. A straightforward strategy is to apply the adjuster to each decision boundary separately. That is, whenever a prediction approaches a discrete decision threshold, regardless of the number of categories, a higher optimization weight is assigned. The underlying theoretical principle remains consistent with the binary case established in Section 3, as each boundary can be locally treated as a binarization problem.

While Section 4 presents experimental validation using ED as an example task, the proposed BAA is fundamentally applicable to a broader range of discrete prediction tasks. For instance, experimental results on the BSDS500 dataset, which is also used for contour detection and segmentation, implicitly demonstrate its broader potential. However, due to the substantial computational cost required for large-scale experiments³ and the fact that this work primarily aims to establish the theoretical framework rather than exhaustive empirical study, we leave extensive cross-task evaluation for fu-

³The experiments on ED alone took approximately three months with GPUs.

ture research. Nevertheless, given that many structured prediction tasks in computer vision, such as segmentation, object detection, and boundary extraction, can be reformulated in terms of ED, we anticipate that the proposed method holds significant potential beyond.

A limitation of the current self-adjusted BAA framework is that model training must be performed twice to determine the binarization threshold thr , incurring additional computational overhead during optimization, though it does not affect inference efficiency. Furthermore, the optimal decision threshold may vary across dataset partitions or benchmarks, requiring recalibration when transferring the model. This issue, however, is fundamentally induced by dataset-dependent evaluation settings rather than by the BAA framework itself. The self-adaptive threshold selection still provides a practical mechanism for choosing a reasonable threshold.

Another drawback is that the self-estimated threshold may not precisely match the true optimal inference threshold. For example, in the ED task, the ideal threshold based on the ODS metric is obtained by test data, while the pre-trained threshold might be derived from it. Since the optimal threshold is inherently impossible to determine during training, the self-adaptive estimation should be regarded as a practically effective surrogate rather than an exact optimal value. Nevertheless, such a surrogate can also provide a method to estimate the real optimal decision threshold, since the real one is not practically accessible.

In summary, although additional calibration is required and further task-specific validation remains open, the theoretical framework provides a principled foundation for improving optimization–inference alignment across a wide spectrum of discrete decision problems.

6. Conclusion

This paper tackles a fundamental yet underexplored issue occurring in discrete decision machine learning tasks: the misalignment between the continuous-valued outputs optimized during training and the discrete predictions required at inference and evaluation. This discrepancy, often overlooked due to the discontinuity of discretiza-

tion, undermines the alignment between training objectives and final task performance.

To address this, we propose a principled binarization adjustment mechanism that incorporates binarization awareness into the training process. Guided by the Distance Weight Function (DWF), the Binarization-Aware Adjuster (BAA) adaptively modulates each element’s contribution to the loss based on its prediction correctness and confidence. It downweights confidently correct predictions since further optimizing them has little effect on the binary output, while emphasizing ambiguous or misclassified regions that are more critical to the final binarization decision. The resulting adjusted loss function from the BAA generalizes traditional loss formulations and embeds binarization behavior directly into the optimization process. In addition, we introduce a self-adaptive training procedure to dynamically estimate an appropriate binarization threshold for the BAA, further aligning training dynamics with inference behavior. Our method is applied to the edge detection (ED) task, and extensive experiments across representative models and datasets validate its effectiveness and robustness.

In summary, the BAA introduces a theoretically grounded mechanism for bridging continuous optimization and discrete evaluation, with application to the ED task, demonstrating the effectiveness experimentally. And beyond ED task and binarization decision tasks, the principle can inform related discrete structured-prediction tasks, offering a promising direction for broader applications.

References

- [1] K. Nazeri, E. Ng, T. Joseph, F. Qureshi, and M. Ebrahimi. Edgeconnect: Structure guided image inpainting using edge prediction. In *2019 IEEE/CVF International Conference on Computer Vision Workshop (ICCVW)*, pages 3265–3274, 2019.
- [2] R. Muthukrishnan and M. Radha. Edge detection techniques for image segmentation. *International Journal of Computer Science & Information Technology*, 3(6):259, 2011.
- [3] C. H. Zhan, X. H. Duan, S. Y. Xu, Z. Song, and M. Luo. An improved moving object detection algorithm based on frame difference and edge detection. In *Fourth*

- international conference on image and graphics (ICIG 2007)*, pages 519–523. IEEE, 2007.
- [4] J. Kittler. On the accuracy of the sobel edge detector. *Image and Vision Computing*, 1(1):37–42, 1983.
- [5] J. Canny. A computational approach to edge detection. *IEEE Transactions on pattern analysis and machine intelligence*, PAMI-8(6):679–698, 1986.
- [6] M. Pu, Y. Huang, Q. Guan, and H. Ling. Rindnet: Edge detection for discontinuity in reflectance, illumination, normal and depth. In *2021 IEEE/CVF International Conference on Computer Vision (ICCV)*, pages 6859–6868. IEEE Computer Society, oct 2021.
- [7] M. Y. Pu, Y. P. Huang, Y. M. Liu, Q. J. Guan, and H. B. Ling. Edter: Edge detection with transformer. In *Proceedings of the IEEE/CVF conference on computer vision and pattern recognition*, pages 1402–1412, 2022.
- [8] C. x. Zhou, Y. P. Huang, M. C. Xiang, J. H. Ren, H. B. Ling, and J. Zhang. Generative edge detection with stable diffusion. *arXiv preprint arXiv:2410.03080*, 2024.
- [9] Y. F. Ye, K. Xu, Y. H. Huang, R. J. Yi, and Z. P. Cai. Diffusedge: Diffusion probabilistic model for crisp edge detection. In *Proceedings of the AAAI conference on artificial intelligence*, volume 38, pages 6675–6683, 2024.
- [10] H. Shu. Boosting edge detection with pixel-wise feature selection: The extractor-selector paradigm, 2025.
- [11] S. N. Xie and Z. W. Tu. Holistically-nested edge detection. In *Proceedings of the IEEE international conference on computer vision*, pages 1395–1403, 2015.
- [12] B. Cetinkaya, S. Kalkan, and E. Akbas. Ranked: Addressing imbalance and uncertainty in edge detection using ranking-based losses. In *Proceedings of the IEEE/CVF Conference on Computer Vision and Pattern Recognition*, pages 3239–3249, 2024.

- [13] H. Shu. Rethinking edge detection through perceptual asymmetry: The swbce loss, 2025.
- [14] D. Martin, C. Fowlkes, D. Tal, and J. Malik. A database of human segmented natural images and its application to evaluating segmentation algorithms and measuring ecological statistics. In *Proc. 8th Int'l Conf. Computer Vision*, volume 2, pages 416–423, July 2001.
- [15] M. Everingham, L. Van Gool, C. K. I. Williams, J. Winn, and A. Zisserman. The pascal visual object classes (voc) challenge. *International Journal of Computer Vision*, 88(2):303–338, jun 2010.
- [16] T. Y. Lin, M. Maire, S. Belongie, L. Bourdev, R. Girshick, J. Hays, P. Perona, D. Ramanan, C. L. Zitnick, and P. Dollár. Microsoft coco: Common objects in context. In *Computer Vision – ECCV 2014*, pages 740–755. Springer International Publishing, 2014.
- [17] N. N. Silberman, D. Hoiem, P. P. Kohli, and R. Fergus. Indoor segmentation and support inference from rgb-d images. In *European Conference on Computer Vision*, 2012.
- [18] X. Soria, E. Riba, and A. Sappa. Dense extreme inception network: Towards a robust cnn model for edge detection. In *2020 IEEE Winter Conference on Applications of Computer Vision (WACV)*, pages 1912–1921. IEEE Computer Society, mar 2020.
- [19] X. Soria, Y. Li, M. Rouhani, and A. D. Sappa. Tiny and efficient model for the edge detection generalization. In *2023 IEEE/CVF International Conference on Computer Vision Workshops (ICCVW)*, pages 1356–1365. IEEE Computer Society, oct 2023.
- [20] Y. B. Fu and X. J. Guo. Practical edge detection via robust collaborative learning. In *Proceedings of the 31st ACM International Conference on Multimedia*, MM '23, page 2526–2534. Association for Computing Machinery, 2023.

- [21] C. Wang, D. Dai, S. Xia, Y. Liu, and G. Wang. One-stage deep edge detection based on dense-scale feature fusion and pixel-level imbalance learning. *IEEE Transactions on Artificial Intelligence*, 5(01):70–79, jan 2024.
- [22] Hao Shu. Enhancing edge detection by texture handling architecture and noiseless training data. 2025.
- [23] N. C. Rakotonirina and A. Rasoanaivo. Esrgan+ : Further improving enhanced super-resolution generative adversarial network. In *ICASSP 2020 - 2020 IEEE International Conference on Acoustics, Speech and Signal Processing (ICASSP)*, pages 3637–3641, 2020.
- [24] A. Vaswani, N. Shazeer, N. Parmar, J. Uszkoreit, L. Jones, A. N. Gomez, L. Kaiser, and I. Polosukhin. Attention is all you need. In *Advances in Neural Information Processing Systems*, volume 30. Curran Associates, Inc., 2017.
- [25] X. Y. Chen, H. Zheng, Y. M. Li, Y. C. Ma, L. Ma, H. Q. Li, and Y. Fan. Versatile medical image segmentation learned from multi-source datasets via model self-disambiguation. In *Proceedings of the IEEE/CVF Conference on Computer Vision and Pattern Recognition*, pages 11747–11756, 2024.
- [26] D.R. Martin, C.C. Fowlkes, and J. Malik. Learning to detect natural image boundaries using local brightness, color, and texture cues. *IEEE Transactions on Pattern Analysis and Machine Intelligence*, 26(5):530–549, 2004.
- [27] J. J. Lim, C. L. Zitnick, and P. Dollár. Sketch tokens: A learned mid-level representation for contour and object detection. In *Proceedings of the IEEE conference on computer vision and pattern recognition*, pages 3158–3165, 2013.
- [28] P. Arbeláez, M. Maire, C. Fowlkes, and J. Malik. Contour detection and hierarchical image segmentation. *IEEE Transactions on Pattern Analysis and Machine Intelligence*, 33(5):898–916, 2011.
- [29] P. Dollár and C. L. Zitnick. Fast edge detection using structured forests. *IEEE Transactions on Pattern Analysis and Machine Intelligence*, 37(8):1558–1570, 2015.

- [30] X. F. Ren. Multi-scale improves boundary detection in natural images. In *Computer Vision–ECCV 2008: 10th European Conference on Computer Vision, Marseille, France, October 12–18, 2008, Proceedings, Part III 10*, pages 533–545. Springer, 2008.
- [31] Y. Liu, M. M. Cheng, X. W. Hu, K. Wang, and X. Bai. Richer convolutional features for edge detection. In *Proceedings of the IEEE conference on computer vision and pattern recognition*, pages 3000–3009, 2017.
- [32] J. Z. He, S. L. Zhang, M. Yang, Y. H. Shan, and T. J. Huang. Bdcn: Bi-directional cascade network for perceptual edge detection. *IEEE Transactions on Pattern Analysis and Machine Intelligence*, 44(1):100–113, 2022.
- [33] Z. Su, W. Z. Liu, Z. T. Yu, D. W. Hu, Q. Liao, Q. Tian, M. Pietikäinen, and L. Liu. Pixel difference networks for efficient edge detection. In *Proceedings of the IEEE/CVF international conference on computer vision*, pages 5117–5127, 2021.
- [34] X. Soria, A. Sappa, P. Humanante, and A. Akbarinia. Dense extreme inception network for edge detection. *Pattern Recognition*, 139:109461, 2023.
- [35] J. H. Jie, Y. Guo, G. X. Wu, J. M. Wu, and B. J. Hua. Edgenat: Transformer for efficient edge detection. *arXiv preprint arXiv:2408.10527*, 2024.
- [36] R. X. Deng, C. H. Shen, S. J. Liu, H. B. Wang, and X. R. Liu. Learning to predict crisp boundaries. In *Computer Vision – ECCV 2018: 15th European Conference, Munich, Germany, September 8–14, 2018, Proceedings, Part VI*, page 570–586. Springer-Verlag, 2018.
- [37] L. X. Huan, N. Xue, X. W. Zheng, W. He, J. Y. Gong, and G. S. Xia. Unmixing convolutional features for crisp edge detection. *IEEE Trans. Pattern Anal. Mach. Intell.*, 44(10 Part 1):6602–6609, oct 2022.
- [38] K. Chen, J. G. Li, W. Y. Lin, J. See, J. Wang, L. Y. Duan, Z. B. Chen, C. W. He, and J. N. Zou. Towards accurate one-stage object detection with ap-loss.

In *Proceedings of the IEEE/CVF Conference on Computer Vision and Pattern Recognition*, pages 5119–5127, 2019.

Data availability

Codes could be found at <https://github.com/Hao-B-Shu/ES-EES-SWBCE-EBT-BAA>.

Author Contribution

The paper has a unique author.

Funding

No funding.

Declaration of Interests

The author declares no conflict of interest.

7. Supplementary Material

7.1. Evaluations on Relaxed Benchmarks in ED tasks

Tables 4 and 5 present the evaluation results under the traditional relaxed criterion, with the pixel error tolerance ranging from 4.3 to 11.1 pixels, depending on the resolution of the evaluated image, and using NMS.

7.2. Full Data Used in the Ablation Study

Table 6 provides the detailed numerical data used to generate Figure 2 in the ablation study.

Table 4

Results on BRIND and BSDS500 with 4.3-pixel error tolerance and NMS: Notations follow those used in the main-text.

	BRIND		BSDS500	
	ODS	OIS	ODS	OIS
HED (2015)	0.781	0.795	0.613	0.630
HED-BAA-0.7	0.786	0.798	0.618	0.639
HED-BAA-SA	0.781	0.793	0.629	0.642
BDCN (2022)	0.770	0.783	0.609	0.631
BDCN-BAA-0.7	0.778	0.791	0.618	0.634
BDCN-BAA-SA	0.779	0.791	0.622	0.645
Dexi (2023)	0.788	0.800	0.642	0.663
Dexi-BAA-0.7	0.791	0.804	0.648	0.673
Dexi-BAA-SA	0.791	0.803	0.639	0.651
EES3-Double (2025)	0.792	0.804	0.651	0.680
EES3-Double-BAA-0.7	0.797	0.809	0.649	0.670
EES3-Double-BAA-SA	0.797	0.808	0.654	0.663
A-No-BAA	0.683	0.796	0.629	0.651
A-BAA-0.7	0.688	0.801	0.633	0.654
A-BAA-0.7-Improvement	+0.73%	+0.63%	+0.64%	+0.46%
A-BAA-SA	0.687	0.799	0.636	0.650
A-BAA-SA-Improvement	+0.59%	+0.38%	+1.11%	-0.15%

Table 5

Results on UDED and BIPED2 with 0.0075 error tolerance and NMS: Notations follow those used in the main-text. A 0.0075 error tolerance corresponds to approximately 11.1-pixel tolerance for BIPED2.

	UDED		BIPED2	
	ODS	OIS	ODS	OIS
HED (2015)	0.806	0.846	0.883	0.890
HED-BAA-0.7	0.818	0.849	0.884	0.892
HED-BAA-SA	0.807	0.843	0.883	0.890
BDCN (2022)	0.786	0.822	0.883	0.890
BDCN-BAA-0.7	0.798	0.828	0.881	0.889
BDCN-BAA-SA	0.801	0.832	0.886	0.893
Dexi (2023)	0.788	0.824	0.887	0.895
Dexi-BAA-0.7	0.801	0.831	0.884	0.892
Dexi-BAA-SA	0.814	0.858	0.886	0.894
EES3-Double (2025)	0.831	0.858	0.888	0.896
EES3-Double-BAA-0.7	0.834	0.863	0.889	0.897
EES3-Double-BAA-SA	0.832	0.859	0.890	0.898
A-No-BAA	0.803	0.838	0.885	0.893
A-BAA-0.7	0.813	0.843	0.885	0.894
A-BAA-0.7-Improvement	+1.25%	+0.60%	+0.00%	+0.11%
A-BAA-SA	0.814	0.848	0.886	0.894
A-BAA-SA-Improvement	+1.37%	+1.19%	+0.11%	+0.11%

Table 6

Hyperparameter Evaluation for thr_{dev} and b : Results are reported on the BRIND dataset under 1-pixel error tolerance without NMS, corresponding to Figure 2. The table lists ODS and OIS scores for various combinations of thr_{dev} and b , while keeping $thr = 0.7$ and $\delta = 1$. Notations follow those in the main-text.

BRIND with 1-pixel error tolerance without NMS		
Hyperparameter: thr - thr_{dev} - δ - b	ODS	OIS
EES3-Double-Adj: 0.7-0.1-1-8	0.686	0.695
EES3-Double-Adj: 0.7-0.2-1-8	0.689	0.698
EES3-Double-Adj: 0.7-0.3-1-8	0.689	0.697
EES3-Double-Adj: 0.7-0.4-1-8	0.689	0.696
EES3-Double-Adj: 0.7-0.5-1-8	0.686	0.694
EES3-Double-Adj: 0.7-0.6-1-8	0.686	0.694
EES3-Double-Adj: 0.7-0.7-1-8	0.687	0.694
EES3-Double-Adj: 0.7-0.1-1-16	0.687	0.695
EES3-Double-Adj: 0.7-0.2-1-16	0.690	0.697
EES3-Double-Adj: 0.7-0.3-1-16	0.688	0.696
EES3-Double-Adj: 0.7-0.4-1-16	0.688	0.696
EES3-Double-Adj: 0.7-0.5-1-16	0.685	0.694
EES3-Double-Adj: 0.7-0.6-1-16	0.687	0.694
EES3-Double-Adj: 0.7-0.7-1-16	0.686	0.694
EES3-Double-Adj: 0.7-0.1-1-32	0.688	0.696
EES3-Double-Adj: 0.7-0.2-1-32	0.690	0.698
EES3-Double-Adj: 0.7-0.3-1-32	0.687	0.695
EES3-Double-Adj: 0.7-0.4-1-32	0.686	0.694
EES3-Double-Adj: 0.7-0.5-1-32	0.687	0.694
EES3-Double-Adj: 0.7-0.6-1-32	0.687	0.695
EES3-Double-Adj: 0.7-0.7-1-32	0.687	0.694